Biomaterials Advances 155 (2023) 213692

Contents lists available at ScienceDirect

Biomaterials Advances

journal homepage: www.journals.elsevier.com/materials-science-and-engineering-c

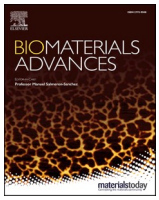

Microfiber-reinforced hydrogels prolong the release of human induced pluripotent stem cell-derived extracellular vesicles to promote endothelial migration

Gerardo Cedillo-Servin [a,b,1], Ana Filipa Louro [c,d,1], Beatriz Gamelas [c,d], Ana Meliciano [c,d], Anne Zijl [a,e], Paula M. Alves [c,d], Jos Malda [a,b,f], Margarida Serra [c,d,1], Miguel Castilho [b,g,h,1,*]

[a] Regenerative Medicine Centre Utrecht, University Medical Center Utrecht, Utrecht, the Netherlands
[b] Department of Orthopedics, University Medical Center Utrecht, Utrecht, the Netherlands
[c] Instituto de Biologia Experimental e Tecnológica (iBET), Oeiras, Portugal
[d] Instituto de Tecnologia Química e Biológica António Xavier, Universidade Nova de Lisboa, Oeiras, Portugal
[e] Faculty of Medicine, Utrecht University, Utrecht, the Netherlands
[f] Department of Equine Sciences, Faculty of Veterinary Medicine, Utrecht University, Utrecht, the Netherlands
[g] Department of Biomedical Engineering, Eindhoven University of Technology, Eindhoven, the Netherlands
[h] Institute for Complex Molecular Systems, Eindhoven University of Technology, Eindhoven, The Netherlands

ARTICLE INFO

Keywords:
Extracellular vesicles
Hydrogel encapsulation
Controlled release
Angiogenesis
Melt electrowriting

ABSTRACT

Extracellular vesicle (EV)-based approaches for promoting angiogenesis have shown promising results. Yet, further development is needed in vehicles that prolong EV exposure to target organs. Here, we hypothesized that microfiber-reinforced gelatin methacryloyl (GelMA) hydrogels could serve as sustained delivery platforms for human induced pluripotent stem cell (hiPSC)-derived EV. EV with 50–200 nm size and typical morphology were isolated from hiPSC-conditioned culture media and tested negative for common co-isolated contaminants. hiPSC-EV were then incorporated into GelMA hydrogels with or without a melt electrowritten reinforcing mesh. EV release was found to increase with GelMA concentration, as 12 % (w/v) GelMA hydrogels provided higher release rate and total release over 14 days *in vitro*, compared to lower hydrogel concentrations. Release profile modelling identified diffusion as a predominant release mechanism based on a Peppas-Sahlin model. To study the effect of reinforcement-dependent hydrogel mechanics on EV release, stress relaxation was assessed. Reinforcement with highly porous microfiber meshes delayed EV release by prolonging hydrogel stress relaxation and reducing the swelling ratio, thus decreasing the initial burst and overall extent of release. After release from photocrosslinked reinforced hydrogels, EV remained internalizable by human umbilical vein endothelial cells (HUVEC) over 14 days, and increased migration was observed in the first 4 h. EV and RNA cargo stability was investigated at physiological temperature *in vitro*, showing a sharp decrease in total RNA levels, but a stable level of endothelial migration-associated small noncoding RNAs over 14 days. Our data show that hydrogel formulation and microfiber reinforcement are superimposable approaches to modulate EV release from hydrogels, thus depicting fiber-reinforced GelMA hydrogels as tunable hiPSC-EV vehicles for controlled release systems that promote endothelial cell migration.

1. Introduction

Extracellular vesicle (EV)-based approaches are being studied for the treatment of heart failure with promising results [1] (reviewed in [2]). However, the therapeutic potential of EV is limited by their stability and their capacity to reach the intended tissue. Extensive pre-clinical data has been gathered on the pharmacokinetics and biodistribution of exogenous EV. In mice models, following intravenous (IV) administration, EV concentration in the bloodstream can decline up to 95 % within the first 5 min [3–5], with EV primarily accumulating in the liver and

* Corresponding author at: Department of Biomedical Engineering, Technical University of Eindhoven, Eindhoven, the Netherlands.
E-mail address: m.dias.castilho@tue.nl (M. Castilho).
[1] Equal contribution.

https://doi.org/10.1016/j.bioadv.2023.213692
Received 28 February 2023; Received in revised form 30 October 2023; Accepted 3 November 2023
Available online 7 November 2023

lungs, and to a lesser extent in the spleen and kidneys. Different delivery routes can alter EV distribution patterns [6], but accumulation in the heart, brain, and skeletal muscle tissue is minimal or absent [7].

The reticuloendothelial system (RES) plays a major role in removing EV from circulation, which explains their rapid accumulation in specific organs (liver, lungs, spleen) that are part of the RES tissue component. Despite displaying some degree of tissue-homing, systemically administered native EV are in its majority incapable of escaping the RES, resulting in off-target effects and low effective doses at the spots of injury. Moreover, though tropism of certain EV types has been observed towards wound sites [8,9], this has not been reported for heart injuries, which renders IV administration inadequate for native EV treatments targeting ischemia and myocardial infarction (MI)-associated heart failure.

The short half-life of EV combined with their fast clearance by the RES hinders therapeutic efficacy and tissue repair. This justifies the use of alternative strategies to localize and/or prolong EV delivery. Approaches have been employed to achieve organ-specific targeting, such as genetic engineering of EV-secreting cells [10–12] or direct chemical modification [13] of the EV membrane [14–16]. Direct injection at the site of injury [17] or incorporation into injectable or adhesive biomaterials has also been shown to improve EV treatment outcomes [18–20].

EV delivery systems such as patches for epicardial application [21] or hydrogels for intramyocardial injection [18,22,23] are generally recognized as appropriate, as they offer control of release within the application site over time. Particularly, hydrogels have been used for several decades in the pharmaceutical industry to prolong drug stability, sustain release, and localize delivery, thereby improving drug bioavailability [25]. Extending the exposure time of the injured tissue to EV has been shown to improve therapeutic outcomes in mice MI models [21,23], which posits hydrogels as promising for applications in delayed release of EV.

Several synthetic or natural derived hydrogels have been tested for EV delivery for tissue regeneration [28–34]. Biocompatible hydrogels such as alginate, collagen, hyaluronic acid, and gelatin methacryloyl (GelMA) were shown to prolong release for up to 21 days [21,35]. Photocrosslinkable GelMA hydrogels have attracted particular interest in regenerative medicine due to their high biocompatibility, degradability, and tunable properties [36]. In GelMA, amino groups on gelatin side chains are replaced by methacryloyl groups, with the degree of functionalization influencing its polymerization and mechanical properties. Modified gelatin can undergo photocrosslinking, while maintaining arginine-glycine-aspartic acid (RGD) motifs and matrix metalloproteinase (MMP) degradation sequences.

Different factors, including polymer concentration, degree of functionalization, photoinitiator type and concentration, light intensity, and exposure duration can be controlled to generate GelMA hydrogels with a wide range of crosslinking densities and stiffness [37]. Physical, chemical, and/or hydrophobic interactions can be exploited to tune hydrogel permeability and the release and transport of loaded biomolecules such as EV. Most studies have focused on describing release profiles of EV-loaded hydrogels [20,32], but there is still much knowledge lacking about the mechanisms underlying EV transport and release from hydrogel or extracellular matrix networks. Only recently, hydrogel stiffness, viscoelastic properties, and EV-hydrogel interactions have been shown to play a significant role in EV transport [39,40], pointing to promising new directions in the design of EV carriers with tissue engineering applications. Fiber-based reinforcements, for instance, have been previously shown to modulate hydrogel mechanical properties, thus representing a streamlined approach that is independent to hydrogel chemistry and crosslinking [41]. In particular, the introduction of microfiber meshes enables precise control over hydrogel mechanics, including stiffness and stress relaxation [42]. Yet, the potential of this orthogonal method to tune hydrogel mechanics has not been previously explored for the release of cell-derived supramolecular therapeutic carriers such as EV.

In this study, pristine and fiber-reinforced GelMA hydrogels were explored as efficient, tunable platforms for sustained and localized delivery of EV for promoting angiogenesis (Fig. 1). To investigate this, EV derived from human induced pluripotent stem cells (hiPSC) were selected as they have been described to promote cardiomyocyte (CM) cell cycle activation and endothelial cell migration and proliferation at higher rates than EV derived from other cells in the cardiac lineage, such as cardiac progenitors and mature or immature CM [43,44]. These initial findings suggest that hiPSC-derived EV (hiPSC-EV) trigger key responses for cardiac regeneration such as endothelial migration and, thus, have greater potential in EV-based therapies. Thus, after being isolated and characterized, hiPSC-EV were labelled with PKH26 and incorporated into GelMA hydrogels at different precursor macromer concentrations, with or without melt-electrowritten microfiber meshes. EV release profiles and stability were investigated *in vitro* over two weeks and modelled to identify the underlying release mechanisms at play. To study the effect of the mechanical confinement provided by the reinforcing mesh on EV release, pristine and reinforced hydrogels were tested for stress relaxation under compression. Finally, bioactivity studies were assessed with human umbilical vein endothelial cells (HUVEC) in order to evaluate the angiogenic potential of hiPSC-EV released for 14 days.

2. Materials and methods

2.1. hiPSC culture and medium harvest

hiPSC (IMR90-4 line) were expanded on coated plates (Matrigel® hESC-Qualified Matrix, Corning®), in feeder-free, serum-free, and animal component-free TeSR-E8™ medium (Stemcell Technologies), in a humidified atmosphere at 37 °C and 5 % CO_2, as described previously [43]. Cells tested negative for mycoplasma contamination. Conditioned culture media was harvested once cells reached 100 % confluency, according to Louro et al. [43].

2.2. EV isolation from conditioned culture medium

EV were separated from conditioned culture medium as described elsewhere [43]. Briefly, conditioned culture medium was centrifuged at 2000*g* (5010R centrifuge, Eppendorf) for 10 min at room temperature, and then filtered through 0.45 μm filter units (Nalgene™ Rapid-Flow™, Thermo Fisher Scientific). Filtered supernatants were centrifuged in 30 mL conical open-top polypropylene tubes (Beckman Coulter) at 110,000 g_{max} for 2h45 min at 4 °C (SW 28 rotor, Ultracentrifuge Optima™ LE-80 K, Beckman Coulter). Pellets were resuspended in DPBS and loaded on the bottom of a bottom-up discontinuous OptiPrep™ density gradient (40 %, 20 %, 10 %, 5 %, 0 % (w/v) iodixanol). Gradients were centrifuged at 110,000 g_{max} for 18 h at 4 °C (SW 28.1 rotor, Ultracentrifuge Optima™ LE-80 K, Beckman Coulter). An equal volume of medium (180 mL) was processed per isolation (each isolation corresponding to one biological replicate).

2.3. Nanoparticle analysis

Nanoparticle Tracking Analysis (NTA) was used to measure the size, size distribution, and concentration of EV samples. For each sample, three videos of 60 s were acquired with screen gain 2 and camera level 14, and a syringe pump infusion speed of 40 on a Nanosight NS300 (Malvern Instruments Ltd.), equipped with a 488 nm laser (<55 mW maximum power) and an automatic syringe pump system. Videos were analyzed by NTA software 3.3 with screen gain 10 and detection threshold 3. Samples were diluted with DPBS to fit the optimal range of the NTA software (3×10^8–1×10^9 particle.mL^{-1}). Size and size distributions determined by NTA corresponded to the hydrodynamic diameters of the particles in suspension.

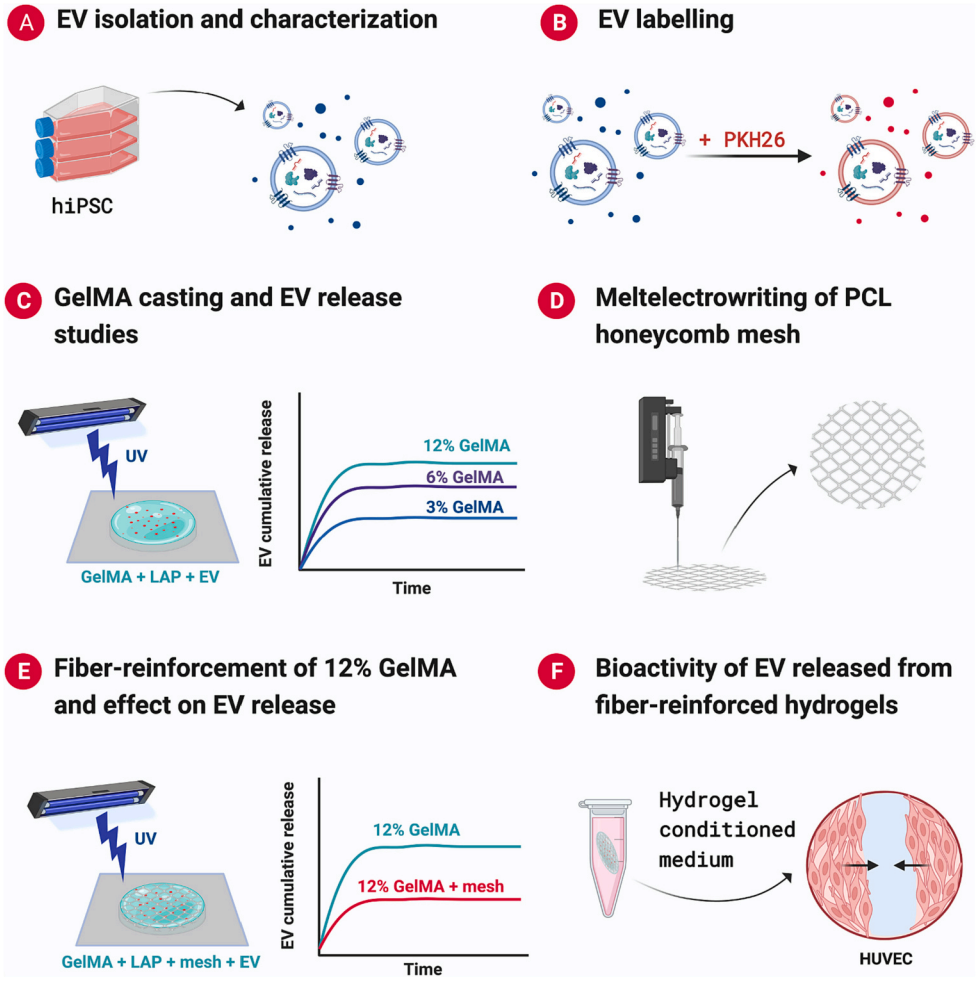

Fig. 1. Overview of the experimental design. (A) EV were isolated from human induced pluripotent stem cell (hiPSC) conditioned cultured medium, characterized, and (B) stained with the lipophilic dye PKH26. (C) Labelled EV were incorporated in different gelatin methacryloyl (GelMA) + LAP formulations and cast on 6 × 2 mm (Ø × h) frames. Gels were characterized in terms of their physical properties, degradation rate, and EV release profile. From the tested formulations, one was selected for further studies. (D) 12 % GelMA hydrogels were cast into hexagonal (honeycomb) meshes produced by MEW. (E) EV release of pristine and mesh-reinforced GelMA hydrogels was assessed. (F) EV-loaded hydrogels were incubated in medium to allow for EV release over 14 days. This hydrogel conditioned medium was used to assess the bioactivity of released EV in human umbilical vein endothelial cells (HUVEC) by assessing EV uptake and wound healing.

2.4. Transmission electron microscopy

Samples were analyzed by TEM to confirm the presence of EV in the isolated gradient fractions and assess EV morphology over 14 days at 37 °C. Briefly, 3 μL of sample were adhered to pre-coated formvar/carbon/glow discharged 100 mesh copper-palladium grids for 20 min. Grids were fixed with 2 % formaldehyde (Science Services) in 0.1 M phosphate buffer for 20 min, washed with sterile water and stained with 2 % uranyl acetate for 5 min. Grids were examined using electron microscopy (FEI Tecnai G2 Spirit BioTWIN operating at 120 keV equipped with an Olympus-SIS Veleta CCD Camera).

2.5. Western blotting

Western blot was performed on EV samples for EV specific markers (CD63 (1:1000, ab59479, Abcam) Flotillin-2 (1:1000, 610838, BD, CD81 (1:1000, EXOAb-CD81A-1, System Biosciences)) and common co-isolated contaminant GM130 (1:250, 610822, BD Pharmingen). Whole cell lysates were analyzed in parallel with EV samples. EV samples were normalized by volume (20 μL of sample per lane), while whole cell lysates were normalized by protein amount (10 μg of protein per lane). Protein concentration of cell lysates was determined by microBCA (ThermoFisher Scientific) according to the manufacturer's instructions. Western blot protocol was performed as previously described [43].

2.6. EV labelling

EV labelling was performed using the PKH26 Red Fluorescent Cell Linker Mini Kit for General Cell Membrane Labelling (Sigma Aldrich). Briefly, each 100 μL of sample were diluted in 100 μL of diluent C, added to 1.5 μL of PKH26 in 100 μL of diluent C, and incubated for 3 min at room temperature. The labelling reaction was stopped by the addition of 100 μL of 0.1 % bovine serum albumin. Labelled vesicles were separated from unbound dye using Exosome Spin Columns (MW 3000, Invitrogen™), as specified by the manufacturer.

2.7. EV stability at 37 °C

Isolated EV samples were resuspended in PBS, aliquoted, and analyzed fresh or stored in a humidified atmosphere at 37 °C, 5 % CO_2. At selected time points (1, 2, 5, 7, and 14 days), an EV aliquot was used for NTA and RNA analysis.

2.8. EV RNA analysis and small RNA relative quantification by RT-qPCR

The decay in EV's bioactive cargo over 14 days was assessed by RT-

qPCR (Real Time quantitative Polymerase Chain Reaction) quantification of small non-coding RNAs formerly identified in hiPSC-EV [43,44]. Briefly, total RNA was isolated from EV samples ($N = 3$ independent EV preparations) using Norgen Biotek Exosomal RNA Isolation kit (Cat. 58,000), according to the manufacturer's instructions. Total RNA was quantified using a Nanodrop-2000c (ThermoFisher Scientific). Small RNA and miRNA were quantified by capillary electrophoresis (Agilent 2100 Bioanalyzer, Agilent Technologies) using the Agilent Small RNA chip, according to the manufacturer's instructions. Reverse transcription of RNA samples was performed with TaqMan™ MicroRNA Reverse Transcription Kit (Applied Biosystems™, Thermo Fisher Scientific) and Custom Taqman™ Small RNA Assays (Applied Biosystems™, ThermoFisher Scientific), according to the manufacturer's protocol. RT-qPCR was performed using the TaqMan™ Fast Advanced Master Mix (Applied Biosystems™, ThermoFisher Scientific) on a LightCycler 480 Instrument II 384-well block (Roche) as previously described [44]. The Cycle threshold (Ct) was determined using the LightCycler 480 software (Roche). Hsa-miR-103a-3p and U6 were selected as endogenous controls based on prior data [44]. Relative changes were analyzed using the ΔΔCt method [45]. Stem-loop primers used for cDNA synthesis and RT-qPCR are available in Table S1 (Supplementary information).

2.9. GelMA synthesis

Gelatin methacryloyl (GelMA) was synthesized as reported previously [46]. Briefly, type-A gelatin from porcine skin (gel strength ~ 300 bloom, 10 % (w/v) in PBS) was reacted with 0.6 g of methacrylic anhydride (92 % purity) per gram of gelatin. The reaction was carried out at 50 °C for 1 h, followed by centrifugation for removal of excess anhydride and dialysis (cellulose membrane, 12–14 kDa cut-off) at 40 °C for 24 h against demineralized water (refreshed twice). The product was freeze-dried and stored at −20 °C. A degree of substitution superior to 80 % was achieved and used for all experiments. All materials for GelMA synthesis were obtained from Sigma Aldrich and used as received.

2.10. EV-loaded and control GelMA hydrogel preparation and casting

hiPSC-EV were incorporated at a concentration of 1.5×10^{10} particle.mL^{-1} (based on NTA) into GelMA + 0.1 % (w/v) Lithium phenyl-2,4,6-trimethylbenzoylphosphinate (LAP, TCI Europe N.V.) photoinitiator solutions to generate 3, 6 and 12 % (w/v) hydrogels. Control hydrogels were prepared with an equal volume of PBS instead of EV sample. The mixtures were pipetted into Teflon molds (Ø = 6 mm × h = 2 mm) and crosslinked under UV light (λ = 365 nm, VL-4.LC, Vilber Lourmat) for 7 min.

2.11. Hydrogel formation analysis

All crosslinked disks were weighed for their initial wet weight ($m_{wet,t=0}$) and three samples were lyophilized to obtain their initial dry weighs ($m_{dry,t=0}$). The remaining samples were incubated in PBS at 37 °C for 24 h, weighed ($m_{wet,t=1}$) freeze-dried and re-weighed ($m_{dry,t=1}$). The sol fraction, swelling ratio (q), and actual macromer fraction (AMF) were determined as follows:

$$\text{sol fraction } (\%) = \left(m_{dry,t=0} - m_{dry,t=1}\right) \times 100 / m_{dry,t=0}$$
$$q = m_{wet,t=1} / m_{dry,t=1}$$
$$\text{AMF} = m_{dry,t=0} / m_{wet,t=0}$$

2.12. Hydrogel degradation studies

Hydrogels were cast, freeze-dried and weighed to determine their initial dry mass ($m_{dry,t=0}$). The remaining hydrogels were placed in 500 μL of PBS at 37 °C. At each time point ($t = x$), hydrogels were removed from PBS, blotted dry, imaged by stereomicroscopy and freeze dried ($m_{dry,t=x}$). Mass loss at each time point was calculated as:

$$\text{Mass loss } (\%) = \left(m_{dry,t=0} - m_{dry,t=x}\right) \times 100 / m_{dry,t=0}$$

2.13. EV release assay and conditioned medium collection

EV-loaded and control hydrogels were cast and incubated at 37 °C either in 500 μL DPBS to assess release, or in 500 μL of endothelial cell culture media for bioactivity screening (complete Endothelial Cell Basal Medium (EBM-2, Lonza) supplemented with EGM™-2 SingleQuots Kit for EV uptake assays or EBM-2 + 0.1 % Fetal Calf Serum (FCS) for wound healing assays) over a 14-day timespan. At each timepoint (4 h, 1, 2, 4, 7, 14 days), 250 μL of DPBS or conditioned culture media were collected and analyzed for quantification of EV release or stored at −80 °C. The removed volume was replenished.

2.14. EV release quantification

Release of PKH26-EV in PBS was quantified by spectrofluorometry in a plate reader (ClarioStar Plus, BMG Labtech), by measuring PKH26 fluorescence signal ($\lambda_{ex} = 520$ nm ± 8, $\lambda_{em} = 567$ nm ± 8, dichroic filter 543.2 nm, fixed gain = 2500). The percentage of EV release was calculated based on a calibration curve performed for each labelled sample.

2.15. Melt electrowriting

Hexagonal-shaped microstructured fiber scaffolds were produced by melt electrowriting (MEW) using a 3D Discovery Evolution system (RegenHU). Granular medical-grade poly(ε-caprolactone) (PCL, Purasorb PC12, Corbion) was melt-extruded in a metallic cartridge at 80 °C through a 24G stainless steel nozzle (inner diameter = 0.3 mm) assisted by an air pressure of 100 kPa and an applied high voltage of 5–6 kV. Hexagonal meshes with a pore side length of 400 μm were obtained after depositing 35 layers of MEW fibers at a collector speed of 6.25 mm.s^{-1} at a collection distance of 2.5 mm between the extrusion nozzle and collector plate. Scanning electron microscopy was performed on sputter-coated PCL meshes (2-nm gold layer, Quorum Q150RS coater) using a Phenom Pro desktop scanning electron microscope (ThermoFisher Scientific. The average fiber diameter was determined to be of 10 μm using ImageJ software. PCL meshes were cut with a biopsy punch (Ø = 6 mm), treated in 1 M aqueous NaOH for 20 min, washed in PBS five times, and then sterilized by immersion in 70 % (v/v) ethanol followed by irradiation in a UV chamber (CL-1000 UVP, Analytik Jena) before use.

2.16. EV-loaded GelMA hydrogel casting on MEW meshes

EV-loaded hydrogel precursor solutions were prepared by dissolving sterile GelMA and LAP stock solutions in sterile PBS for final concentrations of 12 and 0.1 % (w/v), respectively, and incorporating hiPSC-EV at a final concentration of 1.5×10^{10} particle.mL^{-1} (based on NTA). NaOH-treated MEW meshes were placed in Teflon molds (Ø = 6 mm × h = 2 mm), and the EV-loaded precursor solution was pipetted in each well and crosslinked under UV light (λ = 365 nm, VL-4.LC, Vilber Lourmat) for 7 min. Control EV-loaded hydrogels were cast through the same procedure with no MEW mesh.

2.17. Stress relaxation tests

Pristine and MEW mesh-reinforced GelMA hydrogels were tested under uniaxial unconfined compression in a universal mechanical testing machine (MTS Criterion) fitted with a parallel plate system and a 50-N load cell. Hydrogel samples (Ø = 6 mm × h = 2 mm) were tested while submerged in PBS ($n = 6$). Following a 0.1 N pre-load, hydrogel samples were strained to 15 % at a rate of 0.5 % s^{-1} mm/s, followed by a relaxation period of 15 min. Stress-strain curves were calculated from the applied force and displacement data. Stress was defined as the

applied force divided by the cylindrical sample's unloaded cross-sectional area and was processed using a rolling mean filter (window size: 25). To quantify hydrogel relaxation response, a two-term exponential function was fitted to the resulting stress-strain curves using MATLAB software (MathWorks), considering two regimes of stress relaxation: a fast decay regime shortly after peak stress, followed by a slow decay regime that remains until the hydrogel reaches stress equilibrium, as reported previously. The model includes a term for each regime as follows:

$$\sigma = A\ exp\left(-\frac{t}{\tau_1}\right) + C\ exp\left(-\frac{t}{\tau_2}\right)$$

where σ is compressive stress, t is time elapsed since the start of the relaxation period, A and C are coefficients of the fast and slow decay terms, respectively, and τ_1 and τ_2 are the fast and slow relaxation constants, respectively.

2.18. HUVEC culture

HUVEC (#C2517A, Lonza) were cultured according to the manufacturer's specifications. Cells were maintained in complete medium, composed of Endothelial Cell Basal Medium (EBM-2, Lonza) supplemented with Large-vessel endothelial cell growth medium SingleQuots™ Supplements and Growth Factors (Lonza), containing 2 % (v/v) of Fetal Calf Serum (FCS), in a humidified atmosphere at 37 °C in 5 % CO_2, with medium changes every 48 h. HUVEC were used up to passage 6, including.

2.19. EV uptake assay

HUVEC were seeded at a density of 3×10^4 cells per well onto 96-well plates and cultured in complete medium. Twenty-four hours post-seeding, cells were incubated either with free PKH26-EV (3000 particles per cell), or with PKH26-EV hydrogel or control hydrogel conditioned medium. Following a 24 h incubation at 37 °C in 5 % CO_2, cells were washed twice with complete media, to remove any labelled EV not internalized by cells, and subsequently fixed at room temperature for 20 min with 4 % (w/v) paraformaldehyde. Nuclei were counterstained with DAPI (4′,6-Diamidino-2-Phenylindole, Dihydrochloride, ThermoFisher Scientific) reagent. Images were acquired using an inverted fluorescence microscope (Leica DMi8, Leica Systems). Quantification of PKH26-EV positive cells was performed using Fiji software, and calculated as a percentage of DAPI stained nuclei.

2.20. Wound healing assay

HUVEC were seeded at 3×10^4 cells per well onto 96-well ImageLock™ microplates (Essen Bioscience) and incubated for 24 h in complete medium to achieve a confluent cell monolayer. Four hours prior to performing the wound, complete medium was exchanged by starvation medium (ECBM-2 + 0.1 % (v/v) FBS). A 96-pin mechanical wound-making device (WoundMaker™ Essen Bioscience) was used according to the manufacturer's instructions to generate a straight scratch in the confluent cell monolayer, after which cells were washed twice with DPBS to remove cell debris. Equal volumes of EV-hydrogel conditioned medium from each collection time-point were added to the wells, in parallel with conditioned media from the corresponding empty hydrogel controls. Free EV, at a dose of 3000 particles per cell, were also assessed. Positive and negative controls consisted of complete medium and starvation medium, respectively. The plates were placed in an IncuCyte Zoom® system (Essen Bioscience) for automatic monitoring of cell migration. Wound closure was analyzed and calculated using the IncuCyte Zoom® S3 software and the IncuCyte® Scratch Wound Analysis Software Module. The wound closure of test samples was normalized to the respective controls.

2.21. Statistical analysis

Results are plotted as mean ± SD ($N = 3$, except were stated). Statistical significance was tested by one-way ANOVA with Tukey's multiple comparisons test with a single-pooled variance, two-way ANOVA with Tukey's multiple comparisons test, two-tailed unpaired t-test, one-sample t-test, or one-way ANOVA with Dunnett's multiple comparisons test with single-pooled variance, as noted in each case. All statistical analysis was performed with GraphPad Prism v9.

3. Results

3.1. Profiling of in vitro release of hiPSC-EV from pristine and fiber-reinforced GelMA hydrogels

Native hiPSC-EVs, isolated from conditioned media of hiPSC culture (Fig. 1A), had a size range of 50–200 nm, presented a typical cup-shaped morphology, and were positive for EV-associated markers CD63, CD81, TSG101, and Flotilin-2, and negative for common co-isolated contaminant GM130 (Figs. 2A–C; S1). After being labelled with PKH26, hiPSC-EV were incorporated in pristine or fiber-reinforced GelMA hydrogels and characterized in terms of EV release profile and bioactivity (Fig. 1B–F).

In general, the actual macromer fraction (AMF) increased and the sol fraction and swelling ratio decreased with higher GelMA concentration (Fig. S2A–C). Additionally, the degree of hydrogel degradation in an aqueous environment was also concentration-dependent, with 3 % GelMA hydrogels showing higher degradation rates than hydrogels with higher GelMA concentrations (Fig. S2D and E).

GelMA hydrogels displayed a biphasic release kinetics profile with an initial burst followed by a sustained release stage, and the release rate was dependent on the GelMA concentration (Fig. 2D, E). The rapid release (8–21 %) of total EV peaked at 4 h for 12 % GelMA and 24 h for 3 and 6 % GelMA (Fig. 2D and E), after which the rate was reduced but prolonged throughout the experimental period (14 days). At this point, a total of 4.7×10^8 particles (~60 %) had been released from the 12 % GelMA hydrogel, in opposition to 2.7×10^8 particles (~35 %) from the 3 % GelMA hydrogel. Remarkably, 12 % GelMA hydrogels, which present higher macromer fraction, exhibited a faster and higher release of EV compared to 6 % and 3 % hydrogels, the latter showing the lowest release rate.

To understand the EV transport mechanisms involved in GelMA hydrogels and to quantitatively predict the resulting EV release kinetics, we fitted several mathematical models of drug release on the experimental data (Fig. 2F). Based on the comparison of the correlation coefficient (R^2) and of the second-order Akaike Information Criterion (AIC_C), the best fit was selected as that with a R^2 value closest to 1 and a minimal AIC_C value, and thus it was identified to be the Peppas–Sahlin model [48,49]. Analysis of Peppas-Sahlin model parameters revealed that the absolute value of the diffusion constant k_1 was greater than the chain relaxation constant k_2 for all GelMA concentrations tested (Fig. 2G and H). Moreover, the Peppas-Sahlin parameter values showed a close linear relationship with the GelMA concentration within the 3–12 % range studied here (Fig. 2H).

To further modulate EV release kinetics GelMA hydrogels were reinforced with hexagonal PCL meshes (Fig. 3A–C). Stress relaxation analysis showed that the slow stress decay regime predominates in pristine hydrogels with higher GelMA concentration, as observed by significantly higher slow relaxation constants and fast-to-slow coefficient ratios in 12 % GelMA compared to 3 % GelMA (Figs. 3E; S3). Interestingly, the introduction of mesh reinforcement prolonged the slow decay regime in hydrogels with low and high stiffness, namely 3 % and 12 % GelMA, as indicated by significantly higher slow relaxation constants, but not in 6 % GelMA with intermediate stiffness (Fig. 3E). Further, to assess the effect of mesh reinforcement on EV release, the 12 % GelMA concentration was chosen due to its overall higher release rate

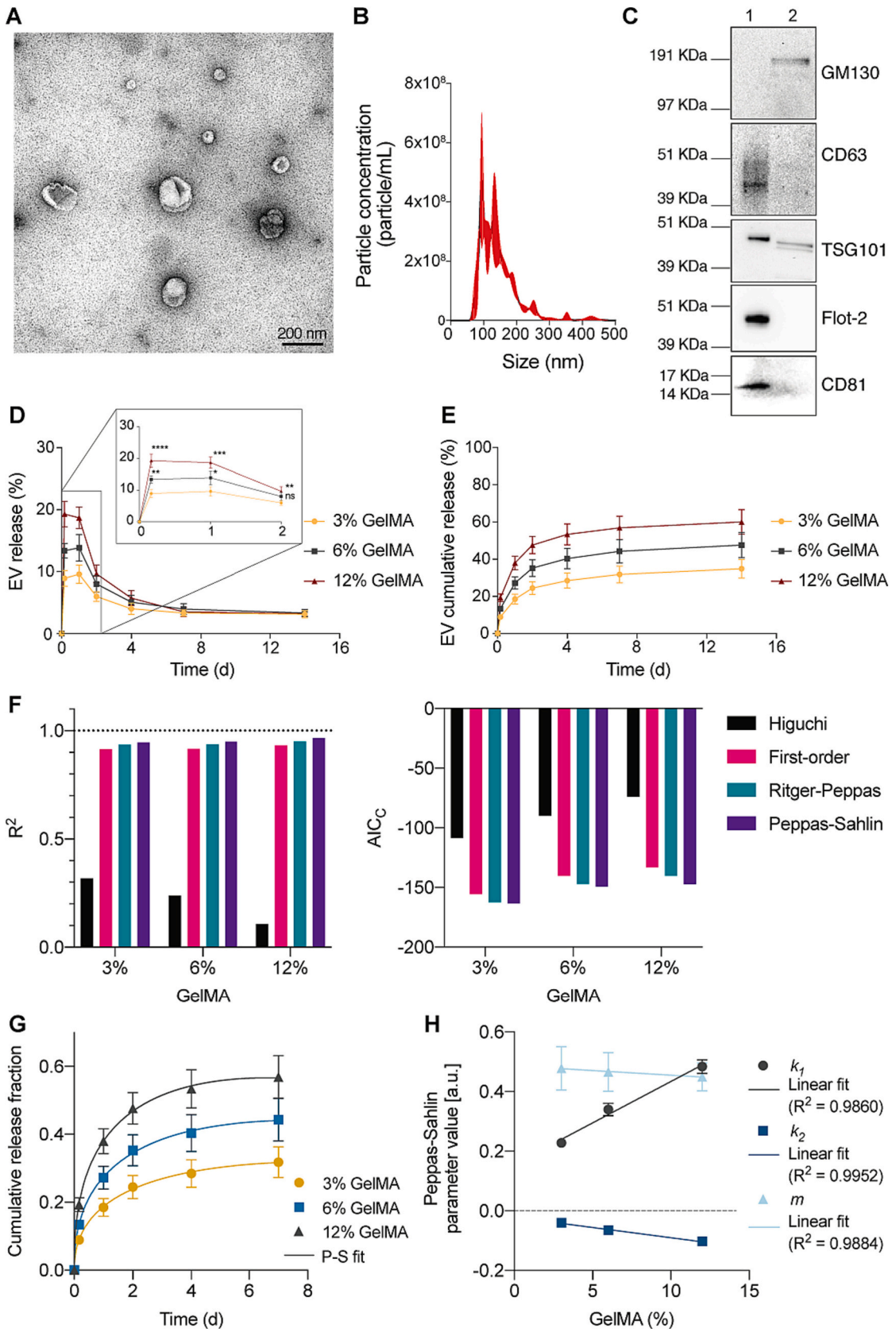

(caption on next page)

Fig. 2. Characterization of hiPSC-EV and release from GelMA hydrogels of different concentrations. (A) Representative negative staining close-up transmission electron microscopy (TEM) image of hiPSC-EV. Scale-bar: 200 nm. (B) Size distribution profile of hiPSC-EV samples analyzed by nanoparticle tracking analysis (NTA). Plotted lines correspond to the averaged size distribution profiles from three EV isolations. Standard deviation is shown in red. (C) Western blot analysis of EV-associated markers CD63, TSG101, Flotillin-2, and CD81, and common co-isolated contaminant GM130. Lane 1 – hiPSC-EV, Lane 2 – whole-cell lysate. (D, E) EV release and cumulative release from 3, 6, and 12 % GelMA hydrogels. In (D) a zoom in of the first 2 days of release is shown. Data represented as mean ± SD ($n = 3$). In (D) significance was tested by a one-way ANOVA with Tukey's multiple comparisons test with a single pooled variance and is shown for GelMA 6 % and 12 % *versus* 3 %. * $p < 0.05$, ** $p < 0.01$, *** $p < 0.001$, **** $p < 0.0001$, n.s. ($p > 0.05$). (F) Modelling of EV release from GelMA hydrogels, evaluated using the R^2 and second-order Akaike Information Criterion (AIC_C) determined for four release models. The Peppas-Sahlin model showed simultaneously the highest R^2 and lowest AIC_C values and hence represented the best fit for the release data. (G) EV-release profiles with a Peppas-Sahlin fit. The continuous lines represent the Peppas-Sahlin model that best fits the cumulative EV release fraction. (H) Peppas-Sahlin model parameters obtained by fitting of the experimental data. Model parameters suggest Fickian diffusion to be the predominant release mechanism. (For interpretation of the references to colour in this figure legend, the reader is referred to the web version of this article.)

in comparison with lower GelMA concentrations (Fig. 2E). The introduction of the meshes resulted in a significant reduction in EV burst, from ~20 % to 4 %, and total release, from ~60 % to 12 % (Fig. 3F).

3.2. hiPSC-EV functionality after release from GelMA hydrogels

To ensure biological activity of hiPSC-EV upon release from GelMA hydrogels, we assessed their uptake (Figs. 4A and B, S4) and ability to induce cell migration (Fig. 4C) in human umbilical vein endothelial cells (HUVEC). PKH26-labelled EV were loaded into 12 % GelMA hydrogels and placed in medium, which was collected at each time-point, and used to supplement HUVEC's cultures. Throughout the 14-day experiment, PKH26-labelled EV were visible inside the cells, although the number of cells positive for EV uptake decreased approximately 60 % over time, correlating with the lower EV release observed for longer time-points (Fig. 4B). Control hydrogels (without loaded EV) did not show any positive PKH26-staining (Fig. 4A).

Further, the hiPSC-EV released from GelMA hydrogels caused a significant increase in cell migration, as measured by the percentage of closure of a scratch created on a HUVEC monolayer, and this effect was only significant in the first 4 h when a burst release occurs, with a similar degree as with free EV (Fig. 4C).

To understand the contribution of EV stability in the observed fast decrease in bioactivity, a stability study was performed on EV at 37 °C, the standard body temperature that EV would encounter *in vivo*. Results showed a gradual reduction in particle concentration over the course of 14 days, accompanied by an increase in smaller particles (<50 nm diameter) concentration, indicating EV degradation (Fig. 5A and B). The notable increase in small particles, lacking signs of typical EV morphology, observed on days 2, 7, and 14 by TEM (Fig. S5) is an additional indicator of EV degradation at 37 °C and corroborates the nanoparticle tracking analysis results. The total RNA content of EV showed a sharp decrease at 24 h, while small RNA concentration remained relatively stable over a 7-day period (Fig. 5C and D). Distinct changes were observed in the levels of specific small RNAs (miR-302c-3p, miR-363c-3p, miR-200c-3p, and piR-36770), which have been previously identified in hiPSC-EV and linked to a promotion of endothelial cell migration through signaling involving PTEN and the PI3K/AKT pathway [43,44]. In particular, piRNA displayed a significant decline in expression, whereas expression of the microRNAs was not significantly affected (Fig. 5D–I).

4. Discussion

The effectiveness of EV-based therapies is limited by their stability and capacity to reach the intended tissue at a correct dose. Conventional systemic infusion can be problematic due to rapid clearance by the RES and low concentrations at the target site, particularly in the heart, which is not a natural accumulation tissue [35]. Therefore, targeting strategies such as modifying the EV surface or direct delivery to the heart are necessary to enhance bioavailability. Additionally, the stability of EV is crucial for developing effective delivery systems, as they can be sensitive to changes in pH, temperature, and mechanical stress. In previous work, we demonstrated the *in vitro* pro-angiogenic effect of hiPSC-EV [43]. Here, we incorporated these EV into photocrosslinkable, fiber-reinforced GelMA hydrogels to enable sustained, localized delivery. We investigated the effect of polymer concentration and crosslinking on hydrogel swelling, degradation, and EV release, while maintaining other variables (degree of polymer functionalization, photoinitiator type and concentration, light intensity, and duration of exposure) constant. We found that a higher macromer concentration resulted in lower hydrogel swelling due to increased crosslinking density, which contributes to hydrogel strength and durability [50]. However, hydrogels with a low macromer percentage (3 % GelMA) were challenging to manipulate and showed faster degradation compared to higher GelMA concentrations.

To achieve sustained EV release, we aimed for a release time frame of 14 days, which is typically the length of an angiogenic response *in vivo* [51–53]. We observed a biphasic release pattern for all the 3 formulations, with an initial burst release within the first 24 h, followed by a sustained release during the following 13 days. By focusing on the largest release timepoint, we found that GelMA concentration had a significant effect on the amount of EV released. Remarkably, EV release was directly proportional to GelMA concentration, with 12 % GelMA resulting in a greater initial and total EV release compared to lower GelMA concentrations, despite having a lower swelling ratio and degradability. To understand this behavior, we analyzed the first 60 % of the EV release curves using the Peppas-Sahlin mathematical model [48,49]. We found that EV release was mainly governed by Fickian diffusion and relaxation of the hydrogel's polymeric chains, [48] and that diffusion played a predominant role in driving release, as indicated by the model parameters $m \approx 0.5$ and $|k_1| > |k_2|$ [48]. Additionally, the model parameters themselves could be fit to GelMA concentration-dependent linear models, which presented high correlation coefficients with respect to experimental data. Therefore, these parameters can be potentially used to determine the GelMA concentration needed to achieve a desired amount of EV release within a specific period.

However, we also found that diffusion is influenced by crosslinking density, with higher crosslinking resulting in decreased water diffusion into and out of the hydrogel matrix, which would oppose the observed EV release kinetics from higher concentration GelMA hydrogels. To explain this effect, we propose two complementary explanations that require further investigation. The first explanation is based on previous work showing that EV transport through the confined environment of a hydrogel matrix is facilitated by high matrix stiffness and matrix stress relaxation, which enables EV to overcome confinement at higher rates [39]. The second hypothesis is that EV electrostatic interactions with the GelMA matrix may play a role, as EV carry a net negative surface charge [56] that is expected to interact with GelMA. Charged proteins, such as b-FGF and BMP-2, have been shown to interact with locally charged regions of GelMA and be retained within hydrogels for sustained periods, suggesting that EV may interact with GelMA in a similar way [57,58].

On the other hand, GelMA has a negative net charge at physiological pH (7.4) due to the prevalence of free carboxyl groups after crosslinking, as amine groups react preferentially in the methacrylation reaction. When GelMA is exposed to a pH higher than its isoelectric point, the

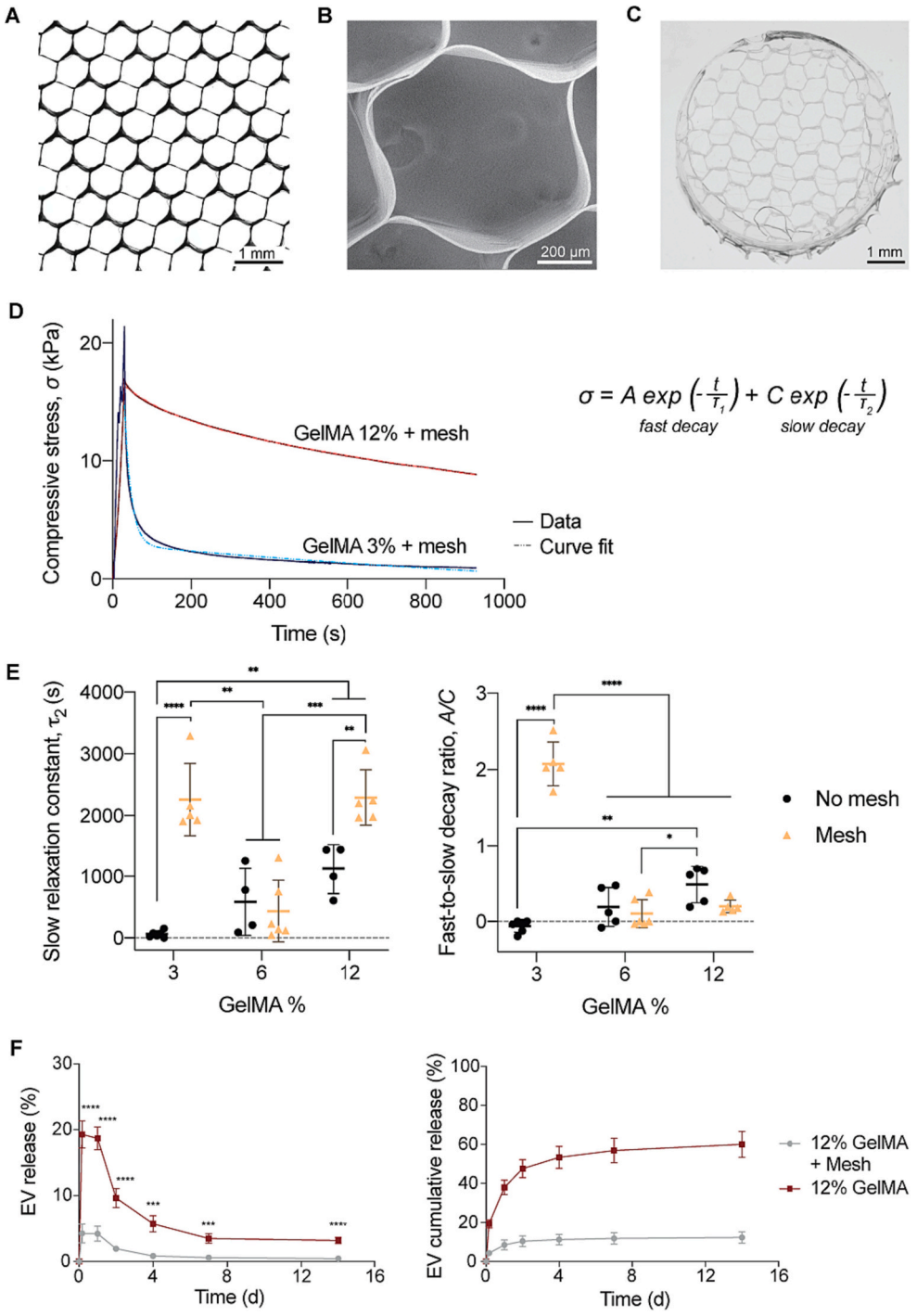

Fig. 3. Stress relaxation and hiPSC-EV release of pristine and MEW mesh-reinforced GelMA hydrogels. (A) Representative transmitted-light image of a hexagonal PCL mesh. (B) Representative SEM image of a hexagonal pore in a PCL fiber mesh. (C) Representative front image of mesh-reinforced 12 % GelMA + 0.1 % LAP hydrogel. (D) Representative stress relaxation curves and exponential fits of mesh-reinforced GelMA hydrogels. (E) Model fit parameters of stress relaxation of pristine and mesh-reinforced GelMA hydrogels. Data presented as mean ± SD ($n \geq 4$); significance was tested by two-way ANOVA with Tukey's multiple comparisons test. (F) Comparison of EV release and cumulative EV release from pristine and mesh-reinforced 12 % GelMA hydrogels. Data presented as mean ± SD ($n = 3$); significance was tested by a two-tailed unpaired *t*-test. * $p < 0.05$, ** $p < 0.01$, *** $p < 0.001$, **** $p < 0.0001$.

proportion of deprotonated carboxyl groups increases, resulting in a more negative net charge. While gelatin type A has an isoelectric point of 7–9 [59], GelMA's isoelectric point is around 5 [60], indicating that GelMA hydrogels have a negative net charge at physiological pH. Increasing polymer concentrations results in higher negative charges inside the hydrogel matrix, which repel negatively charged EV, resulting in faster release profiles.

To enhance the mechanical properties of hydrogels and further modulate EV release, we combined GelMA with a PCL fiber scaffold. We chose a hexagonal structure for the PCL mesh because it guides cardiac cell alignment more effectively and undergoes reversible stretching over larger deformation ranges [61]. Since the PCL meshes have high porosity (>97 %), they were not expected to physically block EV transport through GelMA, but rather modulate EV release by

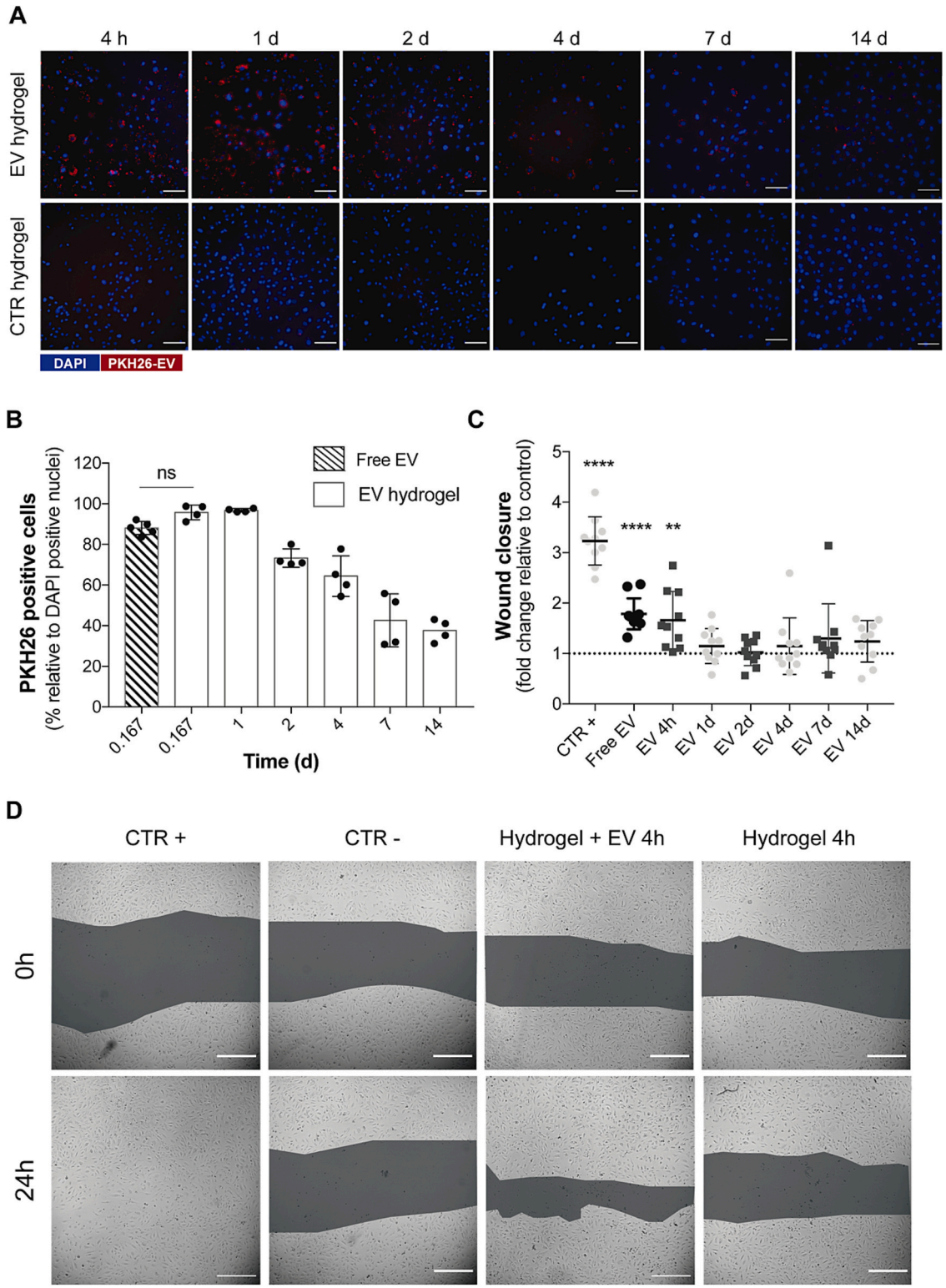

Fig. 4. Bioactivity of EV throughout the release timeframe. A) Representative images of PKH26-EV uptaken by HUVEC during 14 days of EV release. Scale-bar: 100 μm (B) Percentage of HUVEC positive for EV internalization throughout the release timeframe. (C) Effect of EV released at each time-point on HUVEC migration, evaluated by the wound healing assay. Wound closure at 24 h post-scratch is shown relative to negative control. Data shown as average ± SD ($n = 4$). Significance tested by a one-sample *t*-test. ** $p < 0.01$, **** $p < 0.0001$. D) Representative images of cell migration at 0 and 24 h post-scratch of controls and 4 h release samples (EV and empty hydrogel). The dark gray shade corresponds to the wound area. Scale bar: 500 μm. CTR +: positive control (complete medium), CTR −: negative control (starvation medium).

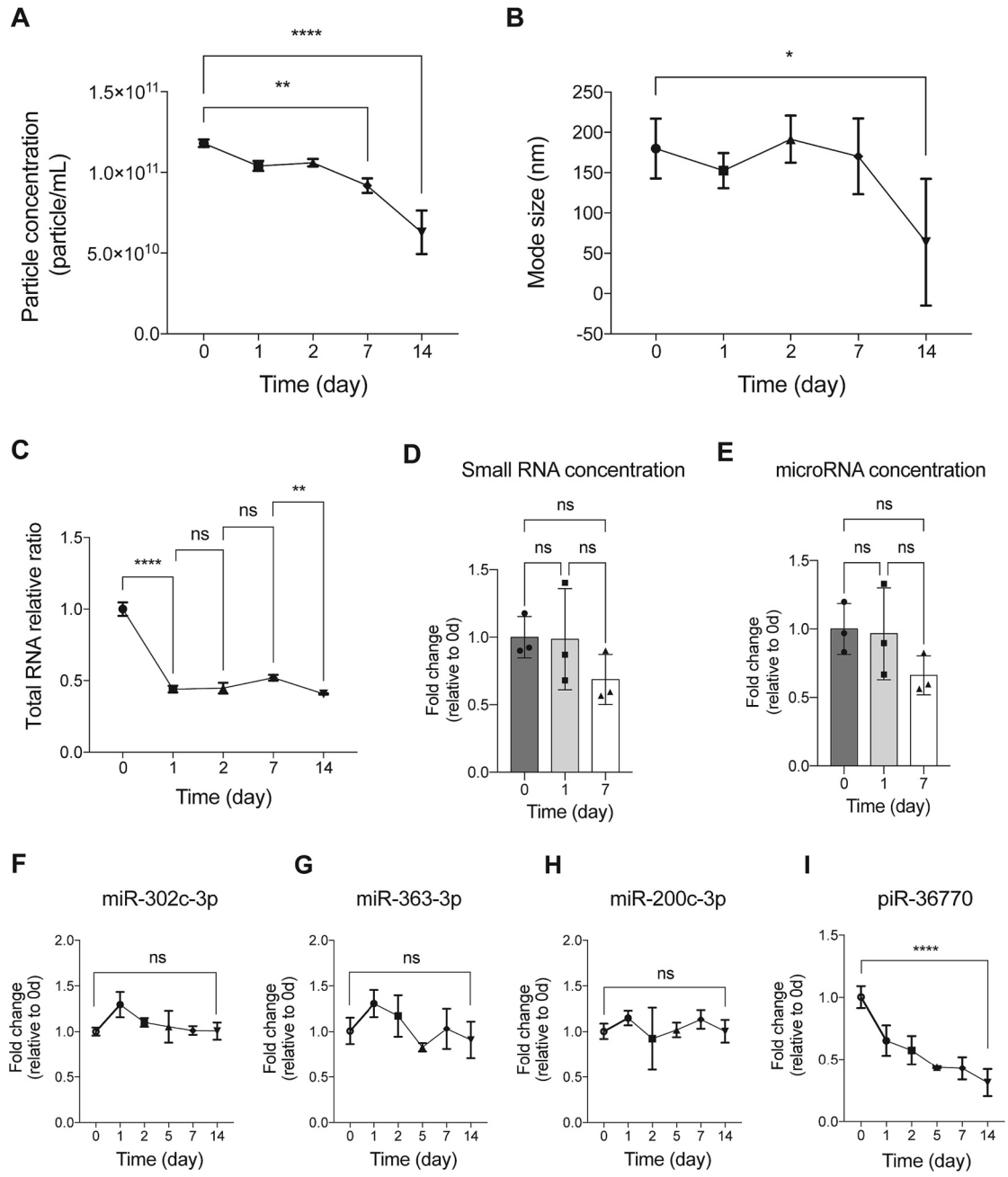

Fig. 5. Stability of EV throughout the release timeframe. EV stability at 37 °C measured by the decrease in (A) particle concentration, (B) mode particle size, and (C) RNA content over 14 days. Fold change in (D) total Small RNA and (E) microRNA concentration in EV over 7 days at 37 °C. (F–I) Relative quantification of small-noncoding RNAs in hiPSC-EV throughout the stability study. Data shown as average ± SD ($n = 3$). Significance was tested by a one-way ANOVA with Dunnett's multiple comparisons test, with a single pooled variance. *$p < 0.05$; ** $p < 0.01$; **** $p < 0.0001$; n.s. $p > 0.05$.

constraining and changing the stress relaxation properties of GelMA hydrogels. The mesh reinforcement prolonged the slow relaxation regime observed in stiffer hydrogels due to mechanical constraints imposed by the mesh. This limits the ability of hydrogel polymer chains to re-organize and accommodate for additional water molecules, thus reducing the swelling ratio, as reported previously [62].

Based on the extent of EV release observed for 12 % GelMA, we chose this formulation for further testing. EV release from mesh-reinforced hydrogels was significantly different from that of pristine hydrogels due to the slower stress relaxation observed in reinforced GelMA. Our findings suggest that mesh reinforcement is a straightforward way to tune EV release independently of hydrogel formulation. Our report here represents the first of its kind in the field of EV encapsulation, since reinforcement with highly porous fiber meshes is presented as an EV release modulating approach that is fully orthogonal to hydrogel chemistry. Additionally, our results highlight the importance of identifying stress relaxation in carrier hydrogels and quantitatively assessing degree of stress relaxation for further modulating EV transport. More detailed investigations into relaxation phenomena like these are necessary to fully leverage the wide range of approaches for tuning hydrogel mechanics and enhancing the potential of hydrogels as EV vehicles with precise release profiles.

We confirmed the bioactivity of hiPSC-EV by evaluating their uptake and ability to promote wound closure *in vitro*. Our results indicate that the EV remain bioactive after casting and photocrosslinking processes, showing similar promotion of endothelial migration compared to free

(non-encapsulated) EV. However, the dose of released EV after the initial burst is likely too low to be effective. In previous studies, research suggested that a dose of 3000 particles per recipient cell is required to trigger pro-angiogenic effects [43]. Considering the total particle payload per hydrogel (7×10^8 particles), the EV release for 12 % GelMA after the first 24 h, and the number of endothelial cells plated per well for the assay ($\sim 3 \times 10^4$ cells), we conclude that after 1 day the released EV were less than half of the required amount to generate an effect (~1430 particles/cell).

Besides dose issues, EV stability throughout the release timeframe also contributes to the limited bioactivity observed. Changes in EV morphology as a result of incubation at physiological temperature were observed by TEM after 2 days at 37 °C. EV stability was further evaluated at the level of particle count and RNA cargo. We employed NanoDrop spectrophotometry to quantify the RNA content and capillary electrophoresis and RT-qPCR to evaluate the levels of small non-coding RNAs previously identified in hiPSC-EV. The combination of these methods allowed to measure the concentrations of small RNAs and miRNAs and relative abundance of target miRNAs/piRNAs and assess the overall RNA content within the EVs. There was a progressive decline in particle concentration, accompanied by a severe reduction in RNA cargo after just 1 day at 37 °C. We probed for specific small non-coding RNAs previously identified in hiPSC-EV and linked to a promotion of endothelial cell migration [43,44]. We observed a significant decay in piR-36770 but not in miR-302c-3p, miR-363-3p, and miR-200c-3p. RNA species in EV are present in distinct relative amounts, with mRNA or mRNA fragments being the more abundant (>50 %) [63,64]. These are generally considered less stable in comparison to other RNA classes, which explains the significant decline in total RNA levels but not in small non-coding RNA levels.

Prior stability studies have evaluated the effect of storage factors such as temperature, pH, time, and freeze-thawing on EV stability. It is generally reported that temperatures above 4 °C cause significant loss of EV particles, RNA, and protein content [65,66]. Although the impact of GelMA on EV stability was not studied, it is clear that once EV are placed at the physiological temperature, they rapidly lose bioactivity. Future studies on EV-loaded biomaterials should take this into account by, for instance, increasing the initial EV burst release while promoting EV retention *in situ*. While literature reports suggest a timeframe varying from 2 days to 3 weeks for EV to induce a relevant cardioprotective effect [35], prolonged EV release may not be feasible for therapeutics employing native vesicles with reduced stability at 37 °C.

Although hydrogel encapsulation has become a promising approach for sustained, localized EV delivery, few studies have investigated the factors that govern EV transport inside a hydrogel matrix (Table S2). This is of particular importance, since EV release can considerably differ from small molecule release due to a greater dependence on hydrogel-associated parameters, such as hydrogel porosity and mechanical properties, as shown here and in previous studies [39]. Overall, our work provides relevant information for the development of biomaterial-based carrier systems for EV therapies, as we showcase two independent strategies to tune EV release, namely, a) hydrogel concentration to modulate crosslink density and hydrogel stiffness, and b) microfiber reinforcement to modulate hydrogel stress relaxation. Additional studies should address some potential pitfalls in release quantification, as here we used PKH26 to track EV. The half-life of lipophilic dyes has been reported to be longer than that of EV, which raises the possibility that at longer time points the remaining dye, and not functional EV, is being analyzed [68]. Other EV tracking methods (*e.g.* ELISA for EV-associated proteins, conjugation of CD63 with fluorescent reporter proteins) should be explored to overcome this bias. Although we have determined diffusion to be an important mechanism in EV release, we can only speculate whether EV/GelMA/PCL interaction mediated by electrostatic charges also plays a significant role in EV retention inside the matrix. Future studies on understanding and modulating these interactions are important to improve control over EV release profiles. Moreover, to confirm and validate the potential of this fiber-reinforced hydrogel-based EV delivery system, future *in vivo* studies in animal models of myocardial infarction should be conducted. These studies should assess the ability of the hydrogel to precisely localize EV delivery within the injured cardiac areas and to evaluate its potential in improving therapeutic effects when compared to conventional intravenous administration or intramyocardial injection.

5. Conclusions

We demonstrate that hiPSC-EV can be incorporated in GelMA + LAP hydrogels without compromising key aspects of their bioactivity in endothelial cells, to achieve a sustained release over 14 days. The release profile can be further tailored by introducing fiber mesh reinforcements, which constrain the hydrogel network, thus limiting stress relaxation and EV diffusion. Mathematical modelling and stress relaxation testing enabled further elucidation of the mechanisms of EV release in pristine and microfiber-reinforced GelMA hydrogels. Overall, our findings characterize hydrogel formulation and fiber reinforcement as two fully orthogonal and superimposable approaches to modulate EV release. This tunable, sustained-release system could contribute to enhance EV retention and improve therapeutic efficacy upon *in vivo* local delivery. Nevertheless, prolonged EV release may be hindered by the short-term stability of native vesicles.

Declaration of competing interest

There are no conflicts of interest related to this manuscript.

Data availability

Data will be made available on request. We have submitted all relevant data on EV source, separation method, and characterization to the EV-TRACK knowledgebase (EV-TRACK ID: EV230026) [Ref. 47].

Acknowledgments

The authors acknowledge Andrei Hrynevich for technical support in melt electrowriting, and A.L. Sousa and E.M. Tranfield from the Electron Microscopy Facility at the IGC for the transmission electron microscopy work. The authors acknowledge financial support from the European Union Horizon 2020 program through project BRAV3 (ID: 874827) and from Fundação para a Ciência e a Tecnologia (FCT) through project EXCELERATE (DOI **10.54499/2022.10467.PTDC**). This work was funded by FCT/Ministério da Ciência, Tecnologia e Ensino Superior (FCT/MCTES, Portugal) through national funds to iNOVA4Health (UIDB/04462/2020 and UIDP/04462/2020) and the Associate Laboratory LS4FUTURE (LA/P/0087/2020). A.F.L. and A.M. were financed by FCT under Grant No. PD/BD/139078/2018 and 2023.04995.BD, respectively. M.C. acknowledges financial support from the Reprint project (OCENW.XS5.161) by The Netherlands Organization for Scientific Research.

Appendix A. Supplementary data

Supplementary data to this article can be found online at https://doi.org/10.1016/j.bioadv.2023.213692.

References

[1] D. Matan, F. Mobarrez, U. Löfström, M. Corbascio, M. Ekström, C. Hage, P. Lyngå, B. Persson, M. Eriksson, C. Linde, H. Persson, H. Wallén, Extracellular vesicles in heart failure – a study in patients with heart failure with preserved ejection fraction or heart failure with reduced ejection fraction characteristics undergoing elective coronary artery bypass grafting, Front. Cardiovasc. Med. 9 (2022), https://doi.org/10.3389/fcvm.2022.952974.

[2] S. Fu, Y. Zhang, Y. Li, L. Luo, Y. Zhao, Y. Yao, Extracellular vesicles in cardiovascular diseases, Cell Death Dis. 6 (2020) 68, https://doi.org/10.1038/s41420-020-00305-y.
[3] M. Morishita, Y. Takahashi, M. Nishikawa, K. Sano, K. Kato, T. Yamashita, T. Imai, H. Saji, Y. Takakura, Quantitative analysis of tissue distribution of the B16BL6-derived exosomes using a streptavidin-lactadherin fusion protein and iodine-125-labeled biotin derivative after intravenous injection in mice, J. Pharm. Sci. 104 (2015) 705–713, https://doi.org/10.1002/JPS.24 251.
[4] M. Morishita, Y. Takahashi, M. Nishikawa, Y. Takakura, Pharmacokinetics of exosomes—an important factor for elucidating the biological roles of exosomes and for the development of exosome-based therapeutics, J. Pharm. Sci. 106 (2017) 2265–2269, https://doi.org/10.1016/J.XPHS.2017.02.030.
[5] Y. Takahashi, M. Nishikawa, H. Shinotsuka, Y. Matsui, S. Ohara, T. Imai, Y. Takakura, Visualization and in vivo tracking of the exosomes of murine melanoma B16-BL6 cells in mice after intravenous injection, J. Biotechnol. 165 (2013) 77–84, https://doi.org/10.1016/J.JBIOTEC.2013.03.013.
[6] O.P.B. Wiklander, J.Z. Nordin, A. O'Loughlin, Y. Gustafsson, G. Corso, I. Mäger, P. Vader, Y. Lee, H. Sork, Y. Seow, N. Heldring, L. Alvarez-Erviti, C.I. Edvard Smith, K. Le Blanc, P. Macchiarini, P. Jungebluth, M.J.A. Wood, S. El Andaloussi, Extracellular vesicle in vivo biodistribution is determined by cell source, route of administration and targeting, J. Extracell. Vesicles 4 (2015) 1–13.
[7] M. Kang, V. Jordan, C. Blenkiron, L.W. Chamley, Biodistribution of extracellular vesicles following administration into animals: a systematic review, J. Extracell. Vesicles 10 (2021), e12085, https://doi.org/10.1002/jev2.12085.
[8] C. Grange, M. Tapparo, S. Bruno, D. Chatterjee, P.J. Quesenberry, C. Tetta, G. Camussi, Biodistribution of mesenchymal stem cell-derived extracellular vesicles in a model of acute kidney injury monitored by optical imaging, Int. J. Mol. Med. 33 (2014) 1055–1063, https://doi.org/10.3892/IJMM.2014.1663.
[9] M.B. Herrera, B. Bussolati, S. Bruno, L. Morando, G. Mauriello-Romanazzi, F. Sanavio, I. Stamenkovic, L. Biancone, G. Camussi, Exogenous mesenchymal stem cells localize to the kidney by means of CD44 following acute tubular injury, Kidney Int. 72 (2007) 430–441, https://doi.org/10.1038/SJ.KI.5002334.
[10] X. Wang, Y. Chen, Z. Zhao, Q. Meng, Y. Yu, J. Sun, Z. Yang, Y. Chen, J. Li, T. Ma, H. Liu, Z. Li, J. Yang, Z. Shen, Engineered exosomes with ischemic myocardium-targeting peptide for targeted therapy in myocardial infarction, J. Am. Heart Assoc. Cardiovasc. Cerebrovasc. Dis. 7 (2018), https://doi.org/10.1161/JAHA.118.008737.
[11] K.I. Mentkowski, J.K. Lang, Exosomes engineered to express a cardiomyocyte binding peptide demonstrate improved cardiac retention in vivo, Sci. Rep. 9 (2019), https://doi.org/10.1038/S41598-019-46407-1.
[12] H. Kim, N. Yun, D. Mun, J.-Y.Y. Kang, S.-H.H. Lee, H.H. Park, H.H. Park, B. Joung, Cardiac-specific delivery by cardiac tissue-targeting peptide-expressing exosomes, Biochem. Biophys. Res. Commun. 499 (2018) 803–808.
[13] A. Vandergriff, K. Huang, D. Shen, S. Hu, M.T. Hensley, T.G. Caranasos, L. Qian, K. Cheng, Targeting regenerative exosomes to myocardial infarction using cardiac homing peptide, Theranostics 8 (2018) 1869, https://doi.org/10.7150/THNO.20524.
[14] M.J. McGuire, K.N. Samli, S.A. Johnston, K.C. Brown, In vitro selection of a peptide with high selectivity for cardiomyocytes in vivo, J. Mol. Biol. 342 (2004) 171–182, https://doi.org/10.1016/J. JMB.2004.06.029.
[15] S. Kanki, D.E. Jaalouk, S. Lee, A.Y.C. Yu, J. Gannon, R.T. Lee, Identification of targeting peptides for ischemic myocardium by in vivo phage display, J. Mol. Cell. Cardiol. 50 (2011) 841–848, https://doi.org/10.1016/J.YJMCC.2011.02.003.
[16] M. Zahid, B.E. Phillips, S.M. Albers, N. Giannoukakis, S.C. Watkins, P.D. Robbins, Identification of a cardiac specific protein transduction domain by in vivo biopanning using a M13 phage peptide display library in mice, PLoS One 5 (2010), e12252, https://doi.org/10.1371/JOURNAL.PONE.0012252.
[17] A.G.E. Ibrahim, K. Cheng, E. Marbán, Exosomes as critical agents of cardiac regeneration triggered by cell therapy, Stem Cell Rep. 2 (2014) 606, https://doi.org/10.1016/J.STEMCR.2014.04.006.
[18] C.W. Chen, L.L. Wang, S. Zaman, J. Gordon, M.F. Arisi, C.M. Venkataraman, J. J. Chung, G. Hung, A.C. Gaffey, L.A. Spruce, H. Fazelinia, R.C. Gorman, S. H. Seeholzer, J.A. Burdick, P. Atluri, Sustained release of endothelial progenitor cell-derived extracellular vesicles from shear-thinning hydrogels improves angiogenesis and promotes function after myocardial infarction, Cardiovasc. Res. 114 (2018) 1029–1040, https://doi.org/10.1093/cvr/cvy067.
[19] K. Zhang, X. Zhao, X. Chen, Y. Wei, W. Du, Y. Wang, L. Liu, W. Zhao, Z. Han, D. Kong, Q. Zhao, Z. Guo, Z. Han, N. Liu, F. Ma, Z. Li, Enhanced therapeutic effects of mesenchymal stem cell-derived exosomes with an injectable hydrogel for hindlimb ischemia treatment, ACS Appl. Mater. Interfaces 10 (2018) 30081–30091, https://doi.org/10.1021/ACSAMI.8B08449.
[20] C. Pezzana, A. Cras, F. Simelière, R. Guesdon, M. Desgres, B.L. Correa, A. Peuffier, V. Bellamy, S. Gouarderes, A. Alberdi, M.-C. Perier, L. Pidial, F. Agnely, A. Bochot, A. Hagège, J.-S. Silvestre, P. Menasché, Biomaterial-embedded extracellular vesicles improve recovery of the dysfunctional myocardium, Biomaterials 291 (2022), 121877, https://doi.org/10.1016/j. biomaterials.2022.121877.
[21] B. Liu, B.W. Lee, K. Nakanishi, A. Villasante, R. Williamson, J. Metz, J. Kim, M. Kanai, L. Bi, K. Brown, G. Di Paolo, S. Homma, P.A. Sims, V.K. Topkara, G. Vunjak-Novakovic, Cardiac recovery via extended cell-free delivery of extracellular vesicles secreted by cardiomyocytes derived from induced pluripotent stem cells, Nat. Biomed. Eng. 2 (2018) 293–303, https://doi.org/10.1038/s41551-018-0229-7.
[22] K. Lv, Q. Li, L. Zhang, Y. Wang, Z. Zhong, J. Zhao, X. Lin, J. Wang, K. Zhu, C. Xiao, C. Ke, S. Zhong, X. Wu, J. Chen, H. Yu, W. Zhu, X. Li, B. Wang, R. Tang, J. Wang, J. Huang, X. Hu, Incorporation of small extracellular vesicles in sodium alginate hydrogel as a novel therapeutic strategy for myocardial infarction, Theranostics 9 (2019) 7403–7416, https://doi.org/10.7150/THNO.32637.
[23] C. Han, J. Zhou, C. Liang, B. Liu, X. Pan, Y. Zhang, Y. Wang, B. Yan, W. Xie, F. Liu, X.Y. Yu, Y. Li, Human umbilical cord mesenchymal stem cell derived exosomes encapsulated in functional peptide hydrogels promote cardiac repair, Biomater. Sci. 7 (2019) 2920–2933, https://doi.org/10.1039/C9BM00101H.
[25] S.W. Kim, Y.H. Bae, T. Okano, Hydrogels: swelling, drug loading, and release, Pharm. Res. 9 (3) (1992) 283–290, https://doi.org/10.1023/A:1015887213431.
[28] O.J. Ramírez, S. Alvarez, P. Contreras-Kallens, N.P. Barrera, S. Aguayo, C.M.A. P. Schuh, Type I collagen hydrogels as a delivery matrix for royal jelly derived extracellular vesicles, Drug Deliv. 27 (2020) 1308–1318, https://doi.org/10.1080/10717544.2020.1818880/SUPPL_FILE/IDRD_A_1818880_SM4346.TIFF.
[29] L.J. Born, S.T. McLoughlin, D. Dutta, B. Mahadik, X. Jia, J.P. Fisher, S.M. Jay, Sustained released of bioactive mesenchymal stromal cell-derived extracellular vesicles from 3D-printed gelatin methacrylate hydrogels, J. Biomed. Mater. Res. A (2022), https://doi.org/10.1002/jbm. a.37362.
[30] H. Hu, L. Dong, Z. Bu, Y. Shen, J. Luo, H. Zhang, S. Zhao, F. Lv, Z. Liu, miR-23a-3p-abundant small extracellular vesicles released from Gelma/nanoclay hydrogel for cartilage regeneration, J. Extracell. Vesicles 9 (2020), https://doi.org/10.1080/20013078.2020.1778883/SUPPL_FILE/ZJEV_A_1778883_SM2167.DOCX.
[31] S. Mardpour, M.H. Ghanian, H. Sadeghi-Abandansari, S. Mardpour, A. Nazari, F. Shekari, H. Baharvand, Hydrogel-mediated sustained systemic delivery of mesenchymal stem cell-derived extracellular vesicles improves hepatic regeneration in chronic liver failure, ACS Appl. Mater. Interfaces 11 (2019) 37421–37433, https://doi.org/10.1021/ACSAMI.9B10126.
[32] E.A. Mol, Z. Lei, M.T. Roefs, M.H. Bakker, M.J. Goumans, P.A. Doevendans, P.Y. W. Dankers, P. Vader, J.P.G. Sluijter, Injectable supramolecular ureidopyrimidinone hydrogels provide sustained release of extracellular vesicle therapeutics, Adv. Healthc. Mater. 8 (2019) 1900847, https://doi.org/10.1002/ADHM.201900847.
[33] N. Nikravesh, O.G. Davies, I. Azoidis, R.J.A. Moakes, L. Marani, M. Turner, C. J. Kearney, N.M. Eisenstein, L.M. Grover, S.C. Cox, Physical structuring of injectable polymeric systems to controllably deliver nanosized extracellular vesicles, Adv. Healthc. Mater. 8 (2019) 1801604, https://doi.org/10.1002/ADHM.201801604.
[34] K. Man, I.A. Barroso, M.Y. Brunet, B. Peacock, A.S. Federici, D.A. Hoey, S.C. Cox, Controlled release of epigenetically-enhanced extracellular vesicles from a GelMA/nanoclay composite hydrogel to promote bone repair, Int. J. Mol. Sci. 23 (2022), https://doi.org/10.3390/ijms23020832.
[35] C. Pezzana, F. Agnely, A. Bochot, J. Siepmann, P. Menasché, Extracellular vesicles and biomaterial design: new therapies for cardiac repair, Trends Mol. Med. 27 (2021) 231–247, https://doi.org/10.1016/j.molmed.2020.10.006.
[36] Y. Piao, H. You, T. Xu, H.-P. Bei, I.Z. Piwko, Y.Y. Kwan, X. Zhao, Biomedical applications of gelatin methacryloyl hydrogels, Eng. Regen. 2 (2021) 47–56, https://doi.org/10.1016/J.ENGREG.2021.03.002.
[37] W. Schuurman, P.A. Levett, M.W. Pot, P.R. van Weeren, W.J.A. Dhert, D. W. Hutmacher, F.P.W. Melchels, T.J. Klein, J. Malda, Gelatin-methacrylamide hydrogels as potential biomaterials for fabrication of tissue-engineered cartilage constructs, Macromol. Biosci. 13 (2013) 551–561, https://doi.org/10.1002/mabi.201200471.
[39] S. Lenzini, R. Bargi, G. Chung, J.W. Shin, Matrix mechanics and water permeation regulate extracellular vesicle transport, Nat. Nanotechnol. 15 (2020) 217–223, https://doi.org/10.1038/s41565-020-0636-2.
[40] S. Lenzini, K. Debnath, J.C. Joshi, S.W. Wong, K. Srivastava, X. Geng, I.S. Cho, A. Song, R. Bargi, J.C. Lee, G.C.H. Mo, D. Mehta, J.-W. Shin, Cell–matrix interactions regulate functional extracellular vesicle secretion from mesenchymal stromal cells, ACS Nano 15 (2021) 17439–17452, https://doi.org/10.1021/acsnano.1c03231.
[41] E.K. Moo, M. Ebrahimi, A. Hrynevich, M. de Ruijter, M. Castilho, J. Malda, R. K. Korhonen, Load-induced fluid pressurisation in hydrogel systems before and after reinforcement by melt-electrowritten fibrous meshes, J. Mech. Behav. Biomed. Mater. 143 (2023), 105941, https://doi.org/10.1016/j.jmbbm.2023.105941.
[42] M. Castilho, V. Mouser, M. Chen, J. Malda, K. Ito, Bi-layered micro-fibre reinforced hydro- gels for articular cartilage regeneration, Acta Biomater. 95 (2019) 297–306, https://doi.org/10.1016/j. actbio.2019.06.030.
[43] A.F. Louro, M.A. Paiva, R.O. Marta, K.A. Kasper, P.M. Alves, P. Gomes-Alves, M. Serra, M.R. Oliveira, K.A. Kasper, P.M. Alves, P. Gomes-Alves, M. Serra, Bioactivity and miRNome profiling of native extracellular vesicles in human induced pluripotent stem cell-cardiomyocyte differentiation, Adv. Sci. (2022), e2104296, https://doi.org/10.1002/ADVS.202104296.
[44] A.F. Louro, N. Virgolini, M.A. Paiva, I.A. Isidro, P.M. Alves, P. Gomes-Alves, M. Serra, Expression of extracellular vesicle PIWI-interacting RNAs throughout hiPSC-cardiomyocyte differentiation, Front. Physiol. 13 (2022), https://doi.org/10.3389/FPHYS.2022.926528.
[45] K.J. Livak, T.D. Schmittgen, Analysis of relative gene expression data using real-time quantitative PCR and the 2(-Delta Delta C(T)) method, Methods 25 (2001) 402–408, https://doi.org/10.1006/METH.2001.1262.
[46] F.P.W. Melchels, W.J.A. Dhert, D.W. Hutmacher, J. Malda, Development and characterization of a new bioink for additive tissue manufacturing, J. Mater. Chem. B 2 (2014) 2282–2289, https://doi.org/10.1039/C3TB21280G.
[47] J. Van Deun, P. Mestdagh, P. Agostinis, Ö. Akay, S. Anand, J. Anckaert, Z. A. Martinez, T. Baetens, E. Beghein, L. Bertier, G. Berx, J. Boere, S. Boukouris, M. Bremer, D. Buschmann, J.B. Byrd, C. Casert, L. Cheng, A. Cmoch, D. Daveloose, E. De Smedt, S. Demirsoy, V. Depoorter, B. Dhondt, T.A.P. Driedonks, A. Dudek, A. Elsharawy, I. Floris, A.D. Foers, K. Gärtner, A.D. Garg, E. Geeurickx,

J. Gettemans, F. Ghazavi, B. Giebel, T.G. Kormelink, G. Hancock, H. Helsmoortel, A.F. Hill, V. Hyenne, H. Kalra, D. Kim, J. Kowal, S. Kraemer, P. Leidinger, C. Leonelli, Y. Liang, L. Lippens, S. Liu, A. Lo Cicero, S. Martin, S. Mathivanan, P. Mathiyalagan, T. Matusek, G. Milani, M. Monguió-Tortajada, L.M. Mus, D. C. Muth, A. Németh, E.N.M. Nolte-'T Hoen, L. O'Driscoll, R. Palmulli, M.W. Pfaffl, B. Primdal-Bengtson, E. Romano, Q. Rousseau, S. Sahoo, N. Sampaio, M. Samuel, B. Scicluna, B. Soen, A. Steels, J.V. Swinnen, M. Takatalo, S. Thaminy, C. Théry, J. Tulkens, I. Van Audenhove, S. Van Der Grein, A. Van Goethem, M.J. Van Herwijnen, G. Van Niel, N. Van Roy, A.R. Van Vliet, N. Vandamme, S. Vanhauwaert, G. Vergauwen, F. Verweij, A. Wallaert, M. Wauben, K.W. Witwer, M.I. Zonneveld, O. De Wever, J. Vandesompele, A. Hendrix, EV-TRACK: transparent reporting and centralizing knowledge in extracellular vesicle research, Nat. Methods 14 (2017) 228–232, https://doi.org/10.1038/nmeth.4185.

[48] N.A. Peppas, J.J. Sahlin, A simple equation for the description of solute release. III. Coupling of diffusion and relaxation, Int. J. Pharm. 57 (1989) 169–172, https://doi.org/10.1016/0378-5173(89)90306-2.

[49] Mathematical models of drug release, in: Strategies to Modify the Drug Release From Pharmaceutical Systems, 2015, pp. 63–86, https://doi.org/10.1016/B978-0-08-100092-2.00005-9.

[50] N. Celikkin, S. Mastrogiacomo, J. Jaroszewicz, X.F. Walboomers, W. Swieszkowski, Gelatin methacrylate scaffold for bone tissue engineering: the influence of polymer concentration, J. Biomed. Mater. Res. A 106 (2018) 201–209, https://doi.org/10.1002/jbm.a.36226.

[51] D. Ribatti, Angiogenesis, in: Brenner's Encyclopedia of Genetics: Second Edition, 2013, pp. 130–132, https://doi.org/10.1016/B978-0-12-374984-0.00065-6.

[52] K. Kobayashi, K. Maeda, M. Takefuji, R. Kikuchi, Y. Morishita, M. Hirashima, T. Murohara, Dynamics of angiogenesis in ischemic areas of the infarcted heart, Sci. Rep. 7 (1) (2017) 1–13, https://doi.org/10.1038/s41598-017-07524-x.

[53] M. Kanazawa, T. Takahashi, M. Ishikawa, O. Onodera, T. Shimohata, G.J. del Zoppo, Angiogenesis in the ischemic core: a potential treatment target? J. Cereb. Blood Flow Metab. 39 (2019) 753, https://doi.org/10.1177/0271678X19834158.

[56] G. Midekessa, K. Godakumara, J. Ord, J. Viil, F. Lättekivi, K. Dissanayake, S. Kopanchuk, A. Rinken, A. Andronowska, S. Bhattacharjee, T. Rinken, A. Fazeli, Zeta potential of extracellular vesicles: toward understanding the attributes that determine colloidal stability, ACS Omega 5 (2020) 16701–16710, https://doi.org/10.1021/ACSOMEGA.0C01582/SUPPL_FILE/AO0C01582_SI_003.AVI.

[57] J.E. Samorezov, E.B. Headley, C.R. Everett, E. Alsberg, Sustained presentation of BMP-2 enhances osteogenic differentiation of human adipose-derived stem cells in gelatin hydrogels, J. Biomed. Mater. Res. A 104 (2016) 1387, https://doi.org/10.1002/JBM.A.35668.

[58] L. Lan, F.R. Tian, D.L. ZhuGe, Q.C. ZhuGe, B.X. Shen, B.H. Jin, J.P. Huang, M. Z. Wu, L.X. Fan, Y.Z. Zhao, H.L. Xu, Implantable porous gelatin microspheres sustained release of bFGF and improved its neuroprotective effect on rats after spinal cord injury, PLoS One 12 (2017), e0173814, https://doi.org/10.1371/JOURNAL.PONE.0173814.

[59] K.B. Djagny, Z. Wang, S. Xu, Gelatin: A Valuable Protein for Food and Pharmaceutical Industries: Review vol. 41, 2010, pp. 481–492, https://doi.org/10.1080/20014091091904.

[60] M. Vigata, C. Meinert, N. Bock, B.L. Dargaville, D.W. Hutmacher, Deciphering the molecular mechanism of water interaction with gelatin methacryloyl hydrogels: role of ionic strength, ph, drug loading and hydrogel network characteristics, Biomedicines 9 (2021), https://doi.org/10.3390/biomedicines9050574.

[61] M. Castilho, A. van Mil, M. Maher, C.H.G. Metz, G. Hochleitner, J. Groll, P. A. Doevendans, K. Ito, J.P.G. Sluijter, J. Malda, Melt electrowriting allows tailored microstructural and mechanical design of scaffolds to advance functional human myocardial tissue formation, Adv. Funct. Mater. 28 (2018) 1803151, https://doi.org/10.1002/adfm.201803151.

[62] B. Kong, Y. Chen, R. Liu, X. Liu, C. Liu, Z. Shao, L. Xiong, X. Liu, W. Sun, S. Mi, Fiber reinforced GelMA hydrogel to induce the regeneration of corneal stroma, Nat. Commun. 11 (1) (2020) 1–12, https://doi.org/10.1038/s41467-020-14887-9.

[63] T. O'Grady, M.S. Njock, M. Lion, J. Bruyr, E. Mariavelle, B. Galvan, A. Boeckx, I. Struman, F. Dequiedt, Sorting and packaging of RNA into extracellular vesicles shape intracellular transcript levels, BMC Biol. 20 (2022) 1–21, https://doi.org/10.1186/S12915-022-01277-4/TABLES/1.

[64] A.O. Batagov, I.V. Kurochkin, Exosomes secreted by human cells transport largely mRNA fragments that are enriched in the 3′-untranslated regions, Biol. Direct 8 (2013) 12, https://doi.org/10.1186/1745-6150-8-12.

[65] M. Lee, J.J. Ban, W. Im, M. Kim, Influence of storage condition on exosome recovery, Biotechnol. Bioprocess Eng. 21 (2016) 299–304, https://doi.org/10.1007/S12257-015-0781-X/METRICS.

[66] Á.M. Lorincz, C.I. Timár, K.A. Marosvári, D.S. Veres, L. Otrokocsi, Á. Kittel, E. Ligeti, Effect of Storage on Physical and Functional Properties of Extracellular Vesicles Derived From Neutrophilic Granulocytes vol. 3, 2014, https://doi.org/10.3402/JEV.V3.25465.

[68] F.J. Verweij, L. Balaj, C.M. Boulanger, D.R.F. Carter, E.B. Compeer, G. D'Angelo, S. El Andaloussi, J.G. Goetz, J.C. Gross, V. Hyenne, E.M. Krämer-Albers, C.P. Lai, X. Loyer, A. Marki, S. Momma, E.N.M. Nolte-'t Hoen, D.M. Pegtel, H. Peinado, G. Raposo, K. Rilla, H. Tahara, C. Théry, M.E. van Royen, R.E. Vandenbroucke, A. M. Wehman, K. Witwer, Z. Wu, R. Wubbolts, G. van Niel, The power of imaging to understand extracellular vesicle biology in vivo, Nat. Methods 18 (2021) 1013–1026, https://doi.org/10.1038/s41592-021-01206-3.